A&A 528, A11 (2011)
DOI: 10.1051/0004-6361/201016301

Astronomy & Astrophysics

A sensitive upper limit to the circular polarization of the Crab nebula at $\lambda 3$ mm

H. Wiesemeyer[1,⋆], C. Thum[1], D. Morris[1], J. Aumont[2], and C. Rosset[3]

[1] Institut de Radioastronomie Millimétrique, 300 rue de la Piscine, 38406 Saint Martin d'Hères, France
e-mail: hwiese@mpifr.de
[2] Institut d'Astrophysique Spatiale, Centre Universitaire d'Orsay, Bât. 121, 91405 Orsay Cedex, France
[3] Astroparticule et Cosmologie, Université Paris-Diderot, Bâtiment Condorcet, 10 rue Alice Domon et Léonie Duquet, 75205 Paris Cedex 13, France

Received 13 December 2010 / Accepted 29 December 2010

ABSTRACT

A new observation of the distribution of the circular polarization over the Crab Nebula supernova remnant yields an upper limit of <0.2% at a radio frequency of 89.2 GHz. This limit is set by the uncertainty in correcting for the instrumental polarization. The raw data were dominated by the conversion of the strong linear polarization to circular in the crosspolarized sidelobes of the 30 m telescope. They were modeled as due to a differential phase gradient between the orthogonally linearly polarized far-field radiation patterns of the two receivers. As the source is tracked these rotate with respect to the radio source distribution on the sky since the telescope has an alt-azimuth mount and a Nasmyth focus. This allows the model to be fit to the raw data and a correction can be made. Our limit of <0.2% is to be compared with <0.03% derived at 610 MHz (Wilson & Weiler 1997, ApJ, 475, 661) and <6% measured at 23 GHz (Wright & Forster 1980, ApJ, 239, 873). These limits are consistent with the polarization expected from an optically thin synchrotron source with the known physical properties of the Crab Nebula. This non-detection does not allow an estimate to be made of the relative contribution to the radio emission from electrons and positrons.

Key words. ISM: supernova remnants – radiation mechanisms: non-thermal – polarization

1. Introduction

The Crab nebula (with its radiosource Tau A) is a plerion-type supernova remnant, consisting of the following components (see Hester 2008, for a review):

1. The pulsar that formed 955 years ago is the engine powering (with a remarkable efficiency, Kennel & Coroniti 1984) the synchrotron emission from the nebula.
2. The pulsar jet transfers this power from the pulsar to the synchrotron nebula, which is confined by the ejecta from the SN explosion. Near the center of the nebula a shock is formed where the jet is thermalized and ultra-relativistic particles are released into the surrounding nebula. The shock appears as features like the X-ray ring (Weisskopf et al. 2000) and the wisps (Scargle 1969) visible in optical and radio images (Bietenholz et al. 2004). There is also an X-ray torus, being magnetically confined as it pushes into the nebula: the magnetic field in the torus is traced by the wisps there (i.e., is toroidal), whereas the magnetic field in the synchrotron nebula has a more complex structure.
3. The synchrotron nebula expands into the swept-up supernova ejecta where another shock forms and Rayleigh-Taylor instabilities lead to the formation of filaments, visible optically.

The work presented here aims at a detection of circular polarization at $\lambda 3$ mm. Several previous observations at lower radio frequency have been reported. Wright & Foster (1980) reported an upper limit of 6% at 23 GHz, and Wilson & Weiler (1997) found an upper limit of 0.03% at 610 MHz. The small circular polarization ($|p_C| \leq 0.3\%$) measured by Martin et al. (1972) in the optical waveband towards the synchrotron nebula is of interstellar origin, namely by dielectric dust particles.

Our measurements of the linear polarization in the synchrotron emission from Tau A and its position angle provide a polarization calibration standard for the high-frequency instrument of the Planck satellite and are published separately (Aumont et al. 2010). Here we present the circular polarization data, aquired at the same time.

2. Observations and data reduction

2.1. Observations

The observations were made with the correlation polarimeter XPOL at the IRAM 30m telescope, from 05 to 09 September 2007 and from 09 to 12 January 2009. The orthogonally polarized receivers were tuned to the frequency of the $HCO^+(J = 1–0)$ transition at 89.2 GHz, and made coherent by a common local oscillator reference (for details see Thum et al. 2008). Our polarimeter allows the measurement of four Stokes parameters simultaneously. The incoming beam from the subreflector is directed into two orthogonally linearly polarized beams, by a wire grid polarizer at 45°. There are two possible orientations of the wires of the grid, either parallel or perpendicular to the plane of incidence. Only in the latter case is the polarization of the reflected beam pure linear, with no crosspolarization. This optimum orientation was only used in 2007, and

⋆ On leave at Max-Planck-Institute for Radio Astronomy, Bonn, Germany.

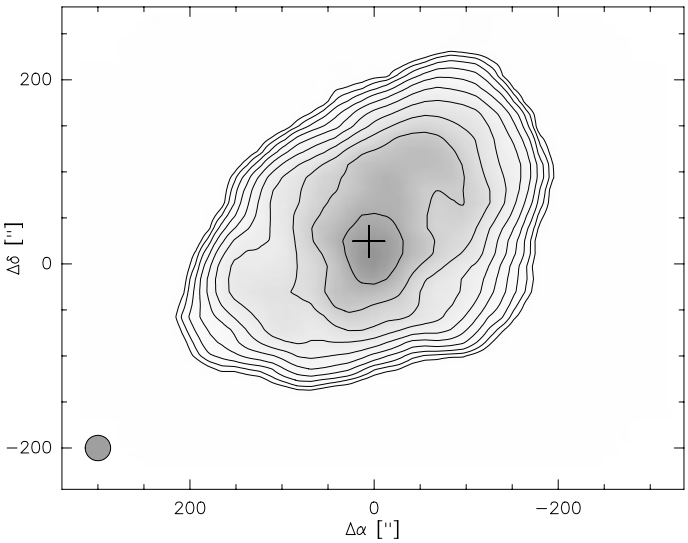

Fig. 1. Stokes I image of Tau A (2009 data). Contours are at $0.2 \times 2^{j-1}$ Jy per beam, with $j = 1$ to 10. *Lowest contour*: 200 mJy (corresponding to $6\sigma_{\rm rms}$). *Highest contour*: 4.5 Jy. The beam's FWHM is indicated in the lower left corner. The cross marks the Pulsar's position. Map center: $\alpha = 05^{\rm h}34^{\rm m}31\overset{\rm s}{.}535$, $\delta = 22°00'27\overset{''}{.}70$ (J2000).

in consequence these observations suffer from fewer systematic errors than the 2009 data.

The images were taken in "on-the-fly" mode, scanning along pairwise orthogonal directions. The half power beam size was $27\overset{''}{.}6$, and the frequency bandpass was 500 MHz wide. The 2009 maps extend to beyond the edge of the synchrotron nebula, such that spatial baselines could be removed from the individual subscans and separate measurements of an emission-free atmospheric reference were unnecessary. In January 2009, the total observing time spent on Tau A was $13\overset{\rm h}{.}5$, to produce in total 40 maps with median system temperature 113 K, yielding an image size of $510'' \times 440''$. The resulting Stokes I image is shown in Fig. 1. The noise level $\sigma_{\rm v}$ (rms) in the corresponding unprocessed Stokes V image is 4.8 mJy per beam.

In September 2007, smaller maps were taken, and the atmospheric emission was removed using a dedicated reference measurement and destriping the Stokes I map with the *Plait* algorithm (Emerson & Gräve 1988). The four final Stokes images were obtained by a weighted mean of the individual images, each weighted by $1/T_{\rm sys}^2$, i.e., the inverse squared system temperature. Such weighting yields an optimum signal-to-noise ratio in the resulting image. A sensitivity of $\sigma_{\rm v} = 3.6$ mJy was achieved, after $10\overset{\rm h}{.}1$ observing time, taking 66 smaller ($455'' \times 330''$) maps, at a median system temperature of 123 K. Because total power fluctuations cancel out in cross correlations, this sensitivity is an order of magnitude below that of the corresponding Stokes I and Q images. More details on the observations and the raw data processing can be found in Aumont et al. (2010).

2.2. Data reduction

2.2.1. Analysis of the instrumental polarization

Owing to the convolution of the intrinsic brightness distribution of the Stokes parameters with the telescope's instrumental response, the Stokes V map, obtained after weighting and gridding the individual maps, is dominated by instrumental artefacts. This can be demonstrated by splitting the set of maps into two subsets whose position angles χ_0 of the vertical direction in the Nasmyth reference frame, after projection onto the sky, are spaced by roughly 90°[1]. The two resulting Stokes V images clearly show different emission patterns, with a circularly polarized flux density ranging between −58 and +50 mJy for the first ensemble of maps, and between −46 and +35 mJy for the second one. This finding immediately shows that the dominant Stokes V signal in the $\lambda 3$ mm continuum emission from Tau A is of instrumental origin: unlike Stokes Q and Stokes U, the Stokes I and V parameters are invariant under rotations of the coordinate system defining the orthogonal componentes of the E vector[2]. Therefore, the Stokes V maps are contaminated by a leakage from linear to circular polarization, while the invariant component is either due to an intrinsic circular polarization, or due to an instrumental generation of Stokes V from Stokes I. This requires crosspolarization in the far-field radiation patterns such as that produced by a non-optimum orientation of the polarizer (for details, see Thum et al. 2008, Appendix). In the case of the 2007 data this effect was negligible. Towards unpolarized sources Stokes V almost vanished ($\leq$0.05%), unlike for the 2009 observations. Generating V from U on the other hand demands a differential phase. In the absence of cross-talk between receivers with orthogonal polarizations and housed in separate dewars (there is no cross talk down to −40 dB, Thum et al. 2008), the major contribution to the instrumental Stokes V is expected to be from small errors in the calibration of the phase difference between the horizontally and vertically polarized signals (since absolute phases do not matter here, in the following phase means "differential phase").

The differential phase can be separated into two components: a small one due to the limited accuracy inherent to our phase calibration scheme (rms better than 1°, Thum et al. 2008), and a systematic contribution owing to the fact that we measure the instrumental phase within the receiver cabin and therefore miss instrumental contributions arising between the phase calibration unit and the far-field. A measurement of the differential phase would only be possible with a celestial point source of strong and well known Stokes U and V continuum signals, which is not available. The data are therefore affected by a direction-dependent differential phase error in the far-field, probably owing to an asymmetric and different illumination of the subreflector by the orthogonally polarized horns, and therefore to a spurious conversion of Stokes U to Stokes V (Müller matrix element $M_{\rm UV}$).

Because correlation polarimetry with orthogonally polarized feed horns yields the Stokes U and V parameters as the real and imaginary part, respectively, of the cross correlation between the input signals, such a phase error affects Stokes V much more than Stokes U, where it is a second order effect. This is so because the circular polarization of virtually all polarized continuum sources on the sky is much weaker than their linear polarization. This can be shown by the following analysis where A denotes the amplitude of the complex cross correlation, ϕ the intrinsic phase of the vertically polarized component of the E vector of the incident wave with respect to the horizontally polarized one and $\Delta\phi$ the phase error. U_0, V_0 are the intrinsic Stokes U and V parameters of the observed object, and $U_{\rm m}$ and $V_{\rm m}$ the measured ones, i.e., including a phase error describing the spurious conversion of Stokes U to Stokes V. The coordinate system for the definition of both the intrinsic and the observed Stokes

[1] The strong linearly polarized flux is then predominantly detected by different receivers in the two subsets.

[2] We adopt the IAU convention, i.e., RHC is positive.

parameters is fixed in the plane of the Nasmyth focus:

$$\begin{aligned} U_\mathrm{m} = A\cos(\phi+\Delta\phi) &= U_0\cos\Delta\phi - V_0\sin\Delta\phi \simeq U_0 \\ \text{for } V_0 &\ll U_0 \text{ and } \Delta\phi \ll 1 \text{ rad}, \\ V_\mathrm{m} = A\sin(\phi+\Delta\phi) &= V_0\cos\Delta\phi + U_0\sin\Delta\phi \\ &\simeq V_0 + U_0\Delta\phi \text{ for } \Delta\phi \ll 1 \text{ rad}. \end{aligned} \quad (1)$$

The result shows that U_m is, to first order, not affected by phase errors, and that the contamination of Stokes V by the phase error is additive. In order to retrieve V_0 from V_m, a model of the distribution of the phase error across the far field beam pattern is thus needed.

2.2.2. A model description of the polarization leakage

In the following, we describe the simplified model for the variation of the differential phase $\Delta\phi$ on the sky and its use to correct the data. It consists of a constant phase offset and a linear variation with angle, assumed due to misalignments on the Nasmyth platform. Here misalignment should be understood as having two components, one being the linear displacements of the receivers from the secondary focus. This produces differential pointing of the main beams on the sky. The second being mispointing of the receivers themselves so that they do not point at the center of the subreflector, and so give rise to asymmetric illuminations of the aperture plane. To a first approximation this will give a linear variation of differential phase between the two orthogonally polarized beams as a function of angle in the far-field.

The relevant measurement equation reads, for a single map j and assuming that the intrinsic (Q_0 and U_0) and measured (Q_m and U_m) Stokes Q and U parameters are stationary while the map is taken (e.g., ignoring parallactic and Nasmyth rotation on a timescale of $0\overset{\mathrm{h}}{.}5$),

$$V_{\mathrm{m},j} = V_0 + \mathcal{B} * U_{0,j}, \quad (2)$$

where $*$ denotes the convolution product and $\mathcal{B}$ the distribution of the phase error $\Delta\phi$ weighted by the telescope's cross-correlation beam pattern. $\mathcal{B}$ is derived from a generic model comprising a constant phase gradient $\nabla\phi$ that results from the unequal illumination of the secondary mirror by the slightly mispointed receivers and therefore assumed to be stationary in the Nasmyth reference frame:

$$\begin{aligned} \mathcal{B}(x_\mathrm{N}, y_\mathrm{N}) &= \mathcal{P}(x_\mathrm{N}, y_\mathrm{N})\Delta\phi(x_\mathrm{N}, y_\mathrm{N}), \\ \text{with } \Delta\phi(x_\mathrm{N}, y_\mathrm{N}) &= \phi_0 + \nabla\phi \cdot \begin{pmatrix} x_\mathrm{N} \\ y_\mathrm{N} \end{pmatrix}. \end{aligned} \quad (3)$$

Here $\mathcal{P}$ is the cross-correlation beam pattern normalized to 1 at peak, given as a Gaussian function of the angular coordinates $(x_\mathrm{N}, y_\mathrm{N})$ in the Nasmyth reference frame,

$$\frac{\Theta^2 \ln \mathcal{P}(x_\mathrm{N}, y_\mathrm{N})}{2\ln 2} = -\sum_{k=1,2}\left[(x_\mathrm{N}-x_{0,k})^2 + (y_\mathrm{N}-y_{0,k})^2\right] \quad (4)$$

with the half-maximum full beamwidth Θ and the offsets of the receivers from the rotation axis, $x_{0,\mathrm{k}}$ and $y_{0,\mathrm{k}}$ (the index $k = 1, 2$ labels the receivers). ϕ_0 is the phase difference between the orthogonal polarizations on the rotation axis defining the origin of the Nasmyth reference frame. The image shown in Fig. 2a is a sensitivity weighted average of the $N_\mathrm{map} = 66$ individual maps observed in 2007, i.e.,

$$\begin{aligned} V_\mathrm{m} &= \sum_{j=1}^{N_\mathrm{map}} w_j (V_0 + \mathcal{B} * U_{0,\mathrm{j}}) = V_0 + \mathcal{B} * \sum_{j=1}^{N_\mathrm{map}} U_{0,\mathrm{j}} w_j \ , \\ \text{with } w_j &= T_{\mathrm{sys,j}}^{-2} \Big/ \sum_{k=1}^{N_\mathrm{map}} T_{\mathrm{sys,k}}^{-2}, \end{aligned} \quad (5)$$

where we assume that V_0 is stationary (see next subsection), i.e. the contamination of Stokes V is given by the convolution of the phase error beam with the Stokes U images, the latter being rotated with respect to the Nasymyth reference system as the source is tracked, and with weights w_j. Because the reference system for the on-the-fly maps is the equatorial system (right ascension and declination offsets $\Delta\alpha$, $\Delta\delta$), it is customary to perform the convolution there rather than in the Nasmyth reference frame. Their respective coordinates are related by the angles η_j (the mean parallactic angle for map j) and $\chi_{0,\mathrm{j}} = \epsilon_j - \eta_j$ (where ϵ_j is the mean elevation for map j),

$$\begin{pmatrix} x_\mathrm{N} \\ y_\mathrm{N} \end{pmatrix} = \begin{pmatrix} -\cos\chi_{0,j} & \sin\chi_{0,j} \\ \sin\chi_{0,j} & \cos\chi_{0,j} \end{pmatrix} \cdot \begin{pmatrix} \Delta\alpha \\ \Delta\delta \end{pmatrix}. \quad (6)$$

The variance χ^2 among the pixels of the difference image

$$\Delta V = V_\mathrm{m} - \mathcal{B} * \sum_{j=1}^{N_\mathrm{map}} U_{0,j} w_j \quad (7)$$

was then minimized by varying four free parameters, namely the phase gradient $(\partial\phi/\partial x, \partial\phi/\partial y)$ and the position of the horizontally polarized reference receiver with respect to the axis on which the phase difference disappears (x_0, y_0), assumed to coincide with the rotation axis (i.e., $\phi_0 = 0$ rad). The differential offset of the receivers was measured independently from pointing observations of strong point sources. Because of the many image processing steps involved in calculating χ^2 for each set of parameters, preference was given to a simulated annealing method (Metropolis algorithm, see Press et al. 1994), using χ^2 as the "energy" to be minimized in the annealing process. This approach is less accurate than other methods, but turned out to be sufficient for our purposes after repeating the minimization of χ^2 with different search options. In an attempt to confirm the fit result, the resulting phase gradient was then fixed, and the receiver offset obtained is within $\simeq 1''$ of the measured one, i.e., rather insensitive to the receiver misalignment within these limits. The results of our analysis are summarized in Table 1. The results of simulations suggest that such effects can be accounted for by an offset of the aperture plane illumination by about 8% of the diameter of the subreflector, or a mis-pointing of the receivers of about $0\overset{\circ}{.}5$. Then $M_\mathrm{UV} \simeq 0.1$. For a given observing epoch, the maximum value of $|p_\mathrm{C}|$ is reproduced by the different approaches. The comparison between the results from 2007 and 2009 shows that the image resulting from the campaign in September 2007 has a lower degree of contamination in Stokes V, owing to the optimum orientation of the beam-splitting grid in 2007, and because the receiver alignment was somewhat better. A map of planet Mars (which is unresolved by the telescope and can safely be considered as unpolarized) confirmed that the instrumental conversion of Stokes I to Stokes V disappeared in the 2007 data ($M_\mathrm{IV} < 3\sigma_\mathrm{rms} = 0.05\%$). The excess of the residual p_C in 2009 stems from the M_IV term not taken into account explicitly, and agrees with the model result from Thum et al. (2008, their Fig. 7) for the non-optimized beam splitter and

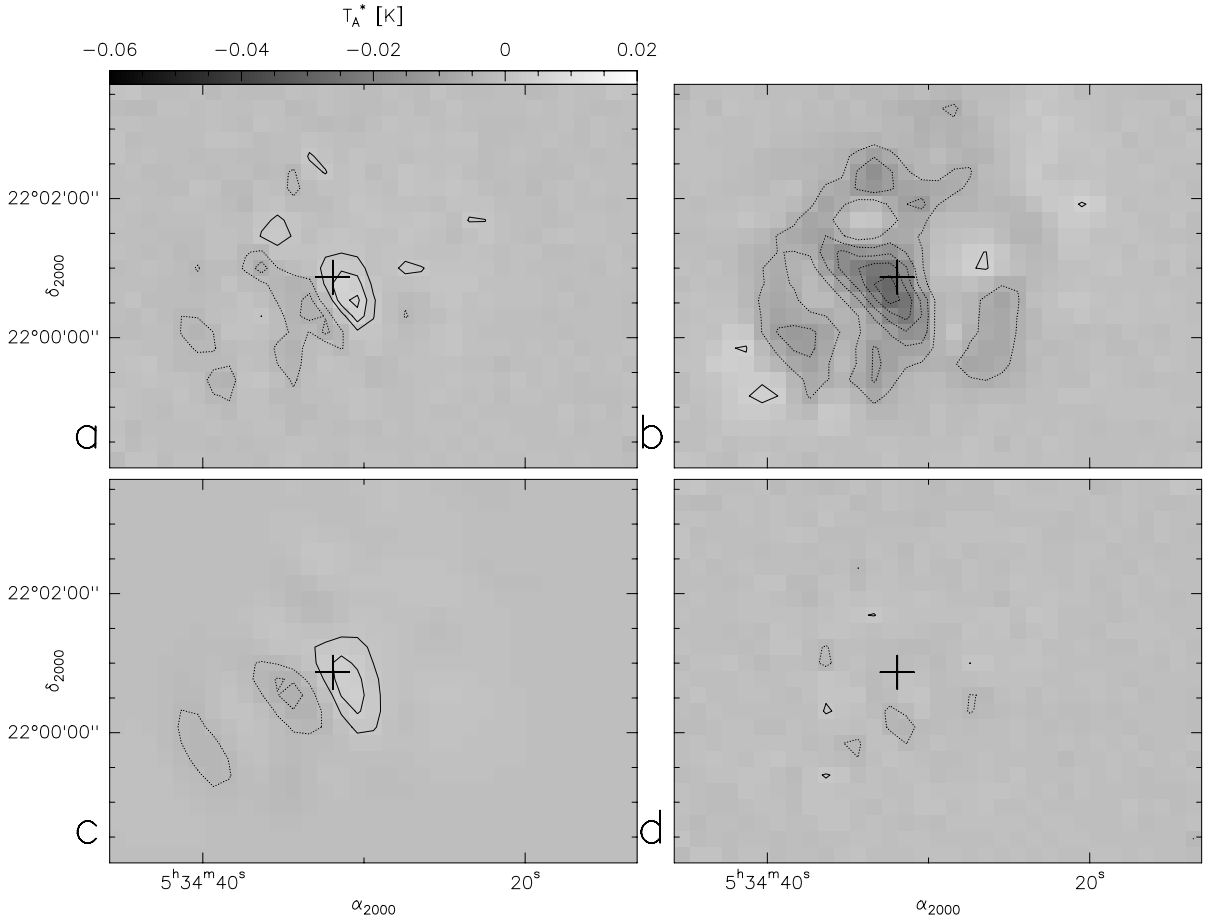

Fig. 2. Demonstration of the image reconstruction process, for the 2007 observations. The cross denotes the position of the pulsar. The grayscale wedge (with T_a^* scale) is for all images. **a)**: raw Stokes V image. Level spacing is 12 mJy/beam (corresponding to about $3\,\sigma_{\rm rms}$); **b)**: average of Stokes U images (Nasmyth reference, level spacing 30 mJy); **c)**: average of scaled Stokes U images after convolution with modeled instrumental response to Stokes V. Contours as in **a)**; **d)**: residual Stokes V image after subtraction of the images averaged in **c)**) from the corresponding Stokes V maps. Level spacing is 12 mJy, about $3\sigma_{\rm rms}$.

0.″8 misalignment. Our analysis requires that the intrinsic polarizations in Stokes U and V, as measured in the equatorial reference frame, remain stationary within either observing campaign. This requirement is fulfilled here: although the outward motion of the radio wisps can be up to ∼0.3c (Bietenholz et al. 2004), it leads, after two months, to a position shift of 1.″6 (for a distance to Tau A of 2 kpc, Trimble 1968), which is still unresolved by our observations.

Figure 2 demonstrates the image reconstruction for the 2007 observations: the raw Stokes V image ($V_{\rm m}$), the mean Stokes U image (weighted average of the $U_{0,j}$), the averaged model images $B * U_{0,j}$ for the parameters minimizing the χ^2 of the difference image ΔV (Eq. (7)), and the resulting reconstructed image of V_0. The dominating antisymmetric pattern of the raw Stokes V image has now disappeared. The noise in the reconstructed Stokes V image of Fig. 2 is about 4 mJy. At the position of the pulsar, we obtain $|p_{\rm C}| \leq 0.20\%$, corresponding to about $3\sigma_{\rm V}$. This upper limit is more sensitive than the 23 GHz limit of Wright & Forster (1980) by a factor of 30.

3. Discussion

Astronomical circular polarization can be produced in two ways, either in the cyclotron- or synchrotron emission process itself that also generates the strong linearly polarized continuum (see e.g., Weiler 1974, for a review), or when the latter crosses a magnetized plasma. Although these processes can be co-spatial, we treat them separately.

3.1. Circular polarization of synchrotron and cyclotron radiation

The absence of a detectable circular polarization in the synchrotron emission from Tau A is not surprising, because the sign of Stokes V depends on whether the velocity vector of an electron emitting synchrotron emission is between the magnetic field direction and the line-of-sight, or outside (i.e., whether the angle ψ between the velocity vector and the line-of-sight is positive or negative). For an isotropic distribution of electrons, there is a small term of the order of $O(\psi^2)$. The linear term in ψ does not cancel either, because the solid angles in which electrons with $\psi > 0$ and $\psi < 0$ radiate are unequal by a factor of $|\psi| \sin\theta$ (Pacholczyk 1977; θ is the angle between the magnetic field direction and the line-of-sight). If self-absorption becomes important, the circular polarization has a sign change at a frequency

$$\nu_{\rm v} = \nu_{\rm m} \left(\frac{\tau_{\rm m}}{\tau_{\rm v}} \right)^{\frac{2}{s+4}}, \qquad (8)$$

where $\nu_{\rm m}$ is the frequency of the maximum of the spectral energy distribution and $\tau_{\rm m}$ is the optical depth at that frequency

Table 1. Summary of fitted parameters. Bold text indicates fixed parameters.

$\nabla\phi$ [°/″]	$(\Delta x, \Delta y)$ [″]	(x_0, y_0) [″]	χ^2 [mK^2]	$\lvert p_C\rvert_{max}$ [%]	$p_{C,pulsar}$ [%]
September 2007					
(−0.02, −0.13)	(+**0.10**, −**0.20**)	(−1.84, +0.59)	1.23	0.7	0.1
(−**0.02**, −**0.13**)	(+0.41, −1.08)	(−2.27, −0.23)	1.20	0.7	0.1
January 2009					
(+0.10, +0.10)	(−**0.30**, −**0.57**)	(−1.60, +0.75)	1.72	1.5	−0.2
(+**0.10**, +**0.10**)	(+0.08, +0.14)	(+0.10, +0.40)	1.47	1.5	−0.1

Notes. Column 1: differential phase gradient, $\nabla\phi = (\partial\phi/\partial x, \partial\phi/\partial y)^T$; Col. 2: receiver misalignment in Nasmyth system; Col. 3: offset of the reference receiver (horizontally polarized) from the rotation axis; Col. 4: χ^2 of the residuals, as defined in Eq. (7); Col. 5: image maximum of p_C (for Stokes I ≥ 150 mK, T_A^*); Col. 6: p_C at pulsar position.

(and τ_ν the optical depth at ν_ν). The spectral index s of the assumed power-law energy distribution of electrons, $N_e(E) = N_e(E_0)(E/E_0)^{-s}$, can be determined from the spectral index of the synchrotron spectrum. The $\lambda 1.3$ mm image of Tau A taken with the same telescope (Bandiera et al. 2002) is too close in frequency to ours and therefore does not allow us to estimate the spectral index, because the accuracy of the flux scale is about 20% at both frequencies. Our flux calibration is consistent with a spectral index between $\lambda 20$ cm and $\lambda 1.3$ mm of $\alpha = -0.28$ to -0.2 (comparing Bandiera et al. 2002 with a $\lambda 20$ cm map, Bietenholz et al. 1997). For frequencies well above the cyclotron turnover (which is below 81.5 MHz, Baars & Hartsuijker 1972), this yields $s = 1 - 2\alpha \simeq 1.5$. The average magnetic field $\langle B\rangle$ has been determined from the break of the radio spectrum, at $\nu \sim 10^{13}$ Hz (Marsden et al. 1984), to be 0.3 mG, corresponding to equipartition between thermal and magnetic pressure. With these values, the sign change of Stokes V due to synchrotron self-absorption occurs at about 0.6 MHz. The intrinsic circular polarization at 89.2 GHz is therefore of the order of 0.01% (using Pacholczyk 1977, Eq. (3.124)). This is for an isotropic distribution of electron energies and optically thin conditions, in a unifrom magnetic field aligned at 45° to the line-of-sight, i.e., an order of magnitude below our upper limit. We note that for a (e^+, e^-) plasma, as usually assumed to be present (Hester 2008, p. 130; Gaensler & Slane 2006) the intrinsic circular polarization would be even smaller. Wilson & Weiler (1997) conclude that their upper limit to $|p_C|$ at 610 MHz is still too high for an estimate of the contribution to the radio emission from positrons with respect to that of electons. The same holds for our upper limit.

3.2. Circular polarization due to radiative transfer effects in a magnetized plasma

Is it conceivable that at high frequency circular polarization can be produced by a more efficient mechanism than the synchrotron emission process itself? The sought-after effect would then be a manifestation of magnetic birefringence. While the Faraday rotation of linear polarization in a magnetized plasma is the most efficient mechanism to convert Stokes parameters into each other, it is only a special case of what is now known as "generalized Faraday effect" (Wilson 1980; Melrose & Robinson 1994). Under the optical thin conditions which apply to the $\lambda 3$ mm emission from Tau A, the transfer of polarized radiation in a collisionless plasma can be described as the motion of a polarization point on the surface of the Poincaré sphere at constant latitude, where the zenith of the coordinate system on the sphere is defined by the natural mode of the medium. The latter depends on the angle ϑ between the magnetic field direction and the line-of-sight. If the natural mode changes along the line-of-sight, the coordinate system changes, too, and the polarization point on the Poincaré sphere follows a complicated trajectory. If the propagation is quasi-longitudinal ($|\vartheta| \ll 1$ rad), the natural mode is circularly polarized, and the radiative transfer leads to the well-known Faraday rotation. If the natural mode is quasi-transversal (i.e. if the line-of-sight crosses a region where ϑ passes through $\pi/2$, a so-called quasi-transversal QT layer), the natural mode is linearly polarized, and the transfer of radiation in such a zone leads to the conversion between linear and circular polarization (dubbed "Faraday pulsation"[3] by Pacholczyk & Swihart 1970; Rosenberg 1972) and leads to a "circular repolarization" of intrinsically linearly polarized radiation (Pacholczyk 1973, considering a cold plasma with an admixture of relativistic electrons). The synchrotron emission observed by us is from a plasma, consisting mainly of relativistic electrons, and for which the natural radiative propagation mode is elliptical (with an axis ratio determined by the number density ratio of cold and relativistic particles, Kennett & Melrose 1998), making the generation of circular polarization easier than in a cold plasma. Detailed calculations for a synchrotron nebula are seemingly yet to be carried out. However, the following estimate may be instructive here. The plasma can be considered stationary with respect to the propagating radiation, since both the plasma frequency $\nu_P = e\sqrt{n_e/\pi m_e} = 324$ kHz and the electron gyrofrequency $\nu_G = eB/2\pi m_e c = 0.84$ kHz are orders of magnitude below our observing frequency of $\nu_{obs} = 89.2$ GHz, for the 0.3 mG magnetic field, and $n_e = 1.3\times10^4$ cm^{-3} (Fesen & Kirshner 1982, from forbidden SII line ratios in the filaments). For such conditions, Segre & Zanza (2001) estimate the production of circular polarization in a QT layer, assuming a constant gradient of the line-of-sight component of the magnetic field, $B\cos\vartheta$, and a constant component B_0 perpendicular to it. Such a situation could apply between the X-ray torus and the body of the synchrotron nebula with their crossed respective fields mentioned in the introduction. For ϑ linearly increasing from 84° to 96° along a line-of-sight element of 0.03 pc (the approximate thickness of the inner X-ray ring seen by Chandra, and of the knots in it, Weisskopf et al. 2000), one obtains $|p_C| \sim 10^{-8}$, which is several orders of magnitude below our upper limit. Circular repolarization is therefore insignificant, because it is of the order of $(\nu_G/\nu_{obs})^2$, whereas Faraday rotation is a first order effect (and most likely, except for some filaments, of interstellar origin, Bietenholz & Kronberg 1990). We infer that the features in the reconstructed Stokes V image (Fig. 2d) are to be attributed to the phase error. They originate most likely from the higher-order effects, neglected in our linear analysis, that can only be

[3] In vapors the effect is known as Voigt effect (Voigt 1898), in liquids as Cotton-Mouton effect.

considered with a detailed model of the response of telescope and receiver cabin optics to partially polarized radiation.

3.3. Circular polarization due to the pulsar emission

Last, but not least, we examine that the Crab pulsar itself does not contribute a strong circularly polarized flux. The optical depth at 89.2 GHz in the foreground synchrotron nebula being negligible, the question arises whether the almost complete circular polarization of the giant pulses (for the Crab pulsar: Hankins et al. 2003; Popov et al. 2006; for PSR B1937+21: Cognard et al. 1996) yields an observable signature at $\lambda 3$ mm. However, it is unlikely that giant pulses contribute to our Stokes V emission, although they constitute the main component of the radio emission from Tau A (Popov et al. 2006): a single giant pulse consists of hundreds of sometimes unresolved nanopulses, but left- and right-circular polarization have a similar occurrence, and the circular polarization therefore tends to cancel out in observations that are unresolved in time. Even if there was a residual Stokes V at radio wavelengths, it would probably be undetectable at mm wavelengths: simultaneous observations of the giant pulses at 0.6 GHz and 1.4 GHz (Sallmen et al. 1999) yield steep spectral indices (between −2.2 and −4.9, average main pulse value ∼4) for them. Extrapolating the typical flux density of a nanopulse of 1000 Jy from 5.5 GHz to 86.2 GHz leaves a flux of 260 mJy, but the time-averaged pulsed flux density would be much lower, at most ∼1 mJy, on top of the synchrotron flux from the nebula towards the pulsar, 5.3 Jy. The sensitivity of our measurements of the fractional circular polarization is 0.1% to 0.2%, still an order of magnitude above the sensitivity needed if the time-averaged pulsed flux density was significantly (i.e., >10%) circularly polarized.

4. Conclusions

This analysis was aimed at an accurate measurement of the circularly polarized component of the $\lambda 3$ mm continuum emission from Tau A. Owing to the strong linear polarization of the emission from the synchrotron nebula, useful results were only obtained after a correction for a differential phase gradient across the far-field beams. Such a gradient most likely arises from the differential illumination of the subreflector by the slightly misaligned, orthogonally polarized receivers whose signals are cross-correlated to detect the linearly and circularly polarized flux. Our corrected data yield an upper limit to the fractional circular polarization towards the Crab pulsar, i.e., near the peak of the radio emission, of 0.2% at 89.2 GHz. This upper limit is not surprising bearing in mind: (1) the weakness of the intrinsic circular polarization of the synchrotron emission at high radio frequency; (2) the disorder and changes in magnetic field direction over the body of the nebula; (3) the high probability that most of the synchrotron radiation comes from a relativistic positron-electron plasma; (4) the low efficiency, at high frequency, of the conversion from linear to circular polarization by radiative transfer effects; (5) the time averaging of the strongly circularly polarized giant pulses from the neutron star. It has been suggested (Kennel & Coroniti 1984) that the radio emission is due to a population of electrons which are accelerated in the filaments which might therefore radiate significant circular polarization. Our sensitivity and angular resolution do not enable a test of this proposition to be made however.

Acknowledgements. We acknowledge the assistance of the technical staff of IRAM Granada, and wish to express our gratitude to Pierre Cox, the director of IRAM, for his grant of observing time, and to the colleagues from the Planck CTWG6 for their help with the observations.

References

Aumont, J., Conversi, L., Thum, C., et al. 2010, A&A, 514, A70
Baars, J. W. M., & Hartsuijker, A. P. 1972, A&A, 17, 172
Bandiera, R., Neri, R., & Cesaroni, R. 2002, A&A, 386, 1044
Bietenholz, M. F., & Kronberg, P. P. 1990, ApJ, 357, L13
Bietenholz, M. F., Kassim, N., Frail, D. A., et al. 1997, ApJ, 490, 291
Bietenholz, M. F., Hester, J. J., Frail, D. A., & Bartel, N. 2004, ApJ, 615, 794
Cocke, W. J., Muncaster, G. W., & Gehrels, T. 1971, ApJ, 169, L119
Cognard, I., Shrauner, J. A., Taylor, J. H., & Thorsett, S. E. 1996, ApJ, 457, L81
Emerson, D. T., & Gräve, R. 1988, A&A, 190, 353
Fesen, R. A., & Kirshner, R. P. 1982, ApJ, 258, 1
Gaensler, B. M., & Slane, P. O. 2006, ARA&A, 44, 17
Hester, J. J. 2008, ARA&A, 46, 127
Kennel, C. F., & Coroniti, F. V. 1984, ApJ, 283, 694
Kennett, M., & Melrose, D. 1998, Publications of the Astronomical Society of Australia, 15, 211
Marsden, P. L., Gillett, F. C., Jennings, R. E., et al. 1984, ApJ, 278, L29
Martin, P. G., Illing, R., & Angel, J. R. P. 1972, MNRAS, 159, 191
Melrose, D. B., & Robinson, P. A. 1994, Proceedings of the Astronomical Society of Australia, 11, 16
Pacholczyk, A. G. 1977, Radio Galaxies, Vol. 89, Pergamon Press International Series on Natural Philosophy
Pacholczyk, A. G. 1973, MNRAS, 163, 29P
Pacholczyk, A. G., & Swihart, T. L. 1970, ApJ, 161, 415
Popov, M. V., Soglasnov, V. A., Kondrat'Ev, V. I., et al. 2006, Astron. Rep., 50, 55
Press, W. H., Teukolsky, S. A., Vetterling, W. T., & Flannery, B. P. 1994, Numerical Recipes in C. The Art of Scienctific Computing, 2nd edn. (Cambridge University Press)
Rosenberg, H. 1972, A&A, 19, 66
Sallmen, S., Backer, D. C., Hankins, T. H., Moffett, D., & Lundgren, S. 1999, ApJ, 517, 460
Scargle, J. D. 1969, ApJ, 156, 401
Segre, S. E., & Zanza, V. 2001, ApJ, 554, 408
Thum, C., Wiesemeyer, H., Paubert, G., Navarro, S., & Morris, D. 2008, PASP, 120, 777
Trimble, V. 1968, AJ, 73, 535
Voigt, W. 1898, Nachr. der K. Gesellsch. der Wiss. zu Göttingen
Weiler, K. W. 1974, Mem. Soc. Astron. Ital., 45, 573
Weisskopf, M. C., Hester, J. J., Tennant, A. F., et al. 2000, ApJ, 536, L81
Wilson, A. S., & Weiler, K. W. 1997, ApJ, 475, 661
Wilson, D. B. 1980, MNRAS, 192, 787
Wright, M. C. H., & Forster, J. R. 1980, ApJ, 239, 873